Article

Cell Reports

LRRTM3 Regulates Excitatory Synapse Development through Alternative Splicing and Neurexin Binding

Graphical Abstract

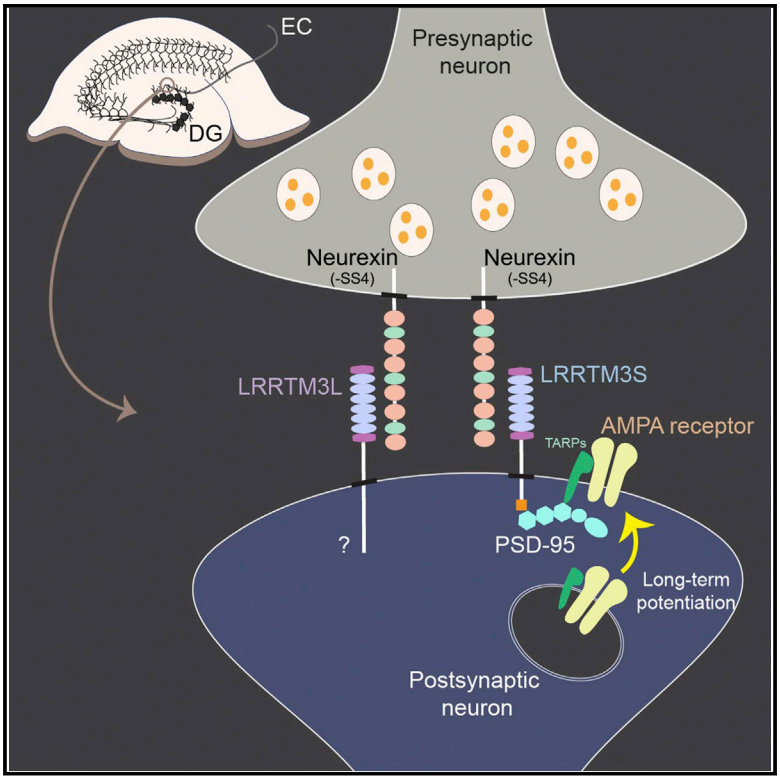

Highlights

- Alternative splicing of *Lrrtm3* and *Lrrtm4* mRNAs produces distinct protein variants
- LRRTM3 is required for DG excitatory synapse development in vitro and in vivo
- LRRTM3 regulates activity-dependent AMPAR surface expression
- Neurexins are universal ligands for all LRRTMs

Authors

Ji Won Um, Tae-Yong Choi, Hyeyeon Kang, ..., Se-Young Choi, Matti S. Airaksinen, Jaewon Ko

Correspondence

jaewonko@yonsei.ac.kr

In Brief

In this study, Um et al. identify leucine-rich repeat transmembrane protein 3 (LRRTM3) as a crucial regulator of excitatory synapse development in dentate gyrus granule neurons. Two different splice variants of LRRTM3 promote excitatory synapse development, but a shorter variant of LRRTM3 that can bind to PSD-95 controls activity-dependent surface expression of the AMPA-type glutamate receptor. Further characterization of LRRTM3-knockout animals revealed that LRRTM3 is required for excitatory synapse structure and function in vivo. Lastly, presynaptic neurexins are required for the LRRTM3 synaptogenic activity that induces presynaptic differentiation, suggesting that LRRTM3 performs synapse-organizing functions that are both redundant and non-redundant relative to those of other LRRTM family members.

Um et al., 2016, Cell Reports *14*, 808–822
February 2, 2016
http://dx.doi.org/10.1016/j.celrep.2015.12.081

OPEN ACCESS
CellPress

Cell Reports
Article

LRRTM3 Regulates Excitatory Synapse Development through Alternative Splicing and Neurexin Binding

Ji Won Um,[1,2,8] Tae-Yong Choi,[3,8] Hyeyeon Kang,[2] Yi Sul Cho,[4] Gayoung Choii,[1] Pavel Uvarov,[5] Dongseok Park,[2] Daun Jeong,[6] Sangmin Jeon,[1] Dongmin Lee,[7] Hyun Kim,[7] Seung-Hee Lee,[6] Yong-Chul Bae,[4] Se-Young Choi,[3] Matti S. Airaksinen,[5] and Jaewon Ko[1,*]

[1]Department of Biochemistry, College of Life Science and Biotechnology, Yonsei University, Seoul 120-749, Korea
[2]Department of Physiology and BK21 PLUS Project to Medical Sciences, Yonsei University College of Medicine, Seoul 120-751, Korea
[3]Department of Physiology, Dental Research Institute, Seoul National University School of Dentistry, Seoul 110-749, Korea
[4]Department of Anatomy and Neurobiology, School of Dentistry, Kyungpook National University, Daegu 700-412, Korea
[5]Department of Anatomy, Faculty of Medicine, University of Helsinki, Helsinki 14, Finland
[6]Department of Biological Sciences, Korea Advanced Institute of Science and Technology (KAIST), Daejeon 305-701, Korea
[7]Department of Anatomy and Neuroscience, Korea 21 Biomedical Science, College of Medicine, Korea University, 126-1, 5-ka, Anam-dong, Seongbuk-gu, Seoul 136-705, Korea
[8]Co-first author
*Correspondence: jaewonko@yonsei.ac.kr
http://dx.doi.org/10.1016/j.celrep.2015.12.081

SUMMARY

The four members of the LRRTM family (LRRTM1-4) are postsynaptic adhesion molecules essential for excitatory synapse development. They have also been implicated in neuropsychiatric diseases. Here, we focus on LRRTM3, showing that two distinct LRRTM3 variants generated by alternative splicing regulate LRRTM3 interaction with PSD-95, but not its excitatory synapse-promoting activity. Overexpression of either LRRTM3 variant increased excitatory synapse density in dentate gyrus (DG) granule neurons, whereas LRRTM3 knockdown decreased it. LRRTM3 also controlled activity-regulated AMPA receptor surface expression in an alternative splicing-dependent manner. Furthermore, *Lrrtm3*-knockout mice displayed specific alterations in excitatory synapse density, excitatory synaptic transmission and excitability in DG granule neurons but not in CA1 pyramidal neurons. Lastly, LRRTM3 required only specific splice variants of presynaptic neurexins for their synaptogenic activity. Collectively, our data highlight alternative splicing and differential presynaptic ligand utilization in the regulation of LRRTMs, revealing key regulatory mechanisms for excitatory synapse development.

INTRODUCTION

Transsynaptic adhesion molecules are central synapse organizers that orchestrate synapse assembly, maturation, specification, and plasticity (Ko et al., 2015a; Missler et al., 2012). Recent research has identified a diverse array of synaptogenic adhesion molecules and investigated their mechanisms of action in different synaptogenesis contexts. Leucine-rich repeat (LRR)-containing transmembrane proteins (LRRTMs), in particular, have emerged as being important for excitatory and inhibitory synapse development. Notably, LRRTMs as well as NGLs (netrin-G ligands), SALMs (synaptic adhesion-like molecules), Slitrks (Slit and Trk-like family), and FLRTs (fibronectin LRR transmembrane protein) were shown to be crucial for various aspects of synapse development (de Wit and Ghosh, 2014; Ko, 2012; Missler et al., 2012; Südhof, 2008; Takahashi and Craig, 2013; Um and Ko, 2013).

The LRRTM family is composed of four members, LRRTM1 to LRRTM4, which are only found in vertebrates (Laurén et al., 2003). They share similar domain architectures consisting of ten LRR domains and a single transmembrane segment but a distinct cytoplasmic stretch that ends with a type I PDZ-binding motif that mediates binding to the excitatory postsynaptic scaffolding protein PSD-95 (Laurén et al., 2003; Linhoff et al., 2009; Siddiqui et al., 2013; Soler-Llavina et al., 2013). All four LRRTMs are able to induce presynaptic differentiation in heterologous synapse-formation assays (de Wit et al., 2009; Ko et al., 2009; Linhoff et al., 2009; Siddiqui et al., 2010), although LRRTM3 displays lower synaptogenic activity relative to other LRRTM family members (de Wit et al., 2009; Linhoff et al., 2009).

Postsynaptic LRRTMs require distinct sets of presynaptic ligands to instruct presynaptic assembly. For example, LRRTM1 and LRRTM2 bind to a subset of presynaptic neurexin splice variants (Ko et al., 2009; Siddiqui et al., 2010), whereas LRRTM4 forms complexes with heparan sulfate proteoglycans and protein tyrosine phosphatase σ (HSPGs/PTPσ) (de Wit and Ghosh, 2014; de Wit et al., 2013; Ko et al., 2015b; Siddiqui et al., 2013). Accordingly, knockdown (KD) of presynaptic neurexins in cultured neurons completely abolishes the synaptogenic activity of LRRTM2, and KD of presynaptic PTPσ significantly decreases the activity of LRRTM4 (Gokce and Südhof, 2013; Ko et al., 2015b). Members of the LRRTM family also exhibit discrete region-specific expression patterns in the hippocampus and cerebellum. In the hippocampus, LRRTM1 and LRRTM2

proteins are strongly expressed in the CA1 region, whereas LRRTM3 and LRRTM4 proteins are prominently expressed in the dentate gyrus (DG) (Laurén et al., 2003; Linhoff et al., 2009; Siddiqui et al., 2013).

A subset of LRRTMs is involved in AMPA (α-amino-3-hydroxy-5-methyl-4-isoxazolepropionic acid) receptor trafficking and function. For example, double KD of LRRTM1 and LRRTM2 in the CA1 hippocampal region of newborn mice reduces AMPA-receptor-mediated excitatory synaptic currents and blocks maintenance of long-term synaptic potentiation (LTP) (Soler-Llavina et al., 2011, 2013). Intriguingly, neurexin binding by LRRTM2 is responsible for LTP maintenance and surface delivery of AMPA receptors during chemical LTP (cLTP) (Soler-Llavina et al., 2013). In a similar vein, presynaptic neurexin-3 controls AMPA receptor surface expression and N-methyl-D-aspartate (NMDA)-receptor-dependent LTP in an alternative-splicing-dependent manner, partly via interactions with LRRTM2 (Aoto et al., 2013). Furthermore, LRRTM4 forms physical complexes with the GluA2 subunit of AMPA receptors and is required for cLTP-induced synaptic surface trafficking of GluA1 subunits (Schwenk et al., 2012; Shanks et al., 2012; Siddiqui et al., 2013).

Analyses of in vivo LRRTM functions in knockout (KO) mice have revealed subtle anatomical and significant functional and behavioral defects. *Lrrtm1*-KO mice display increased VGLUT1 (vesicular glutamate transporter 1) immunofluorescence, altered distribution of synaptic vesicles, and altered hippocampal synapse morphology and density (Linhoff et al., 2009; Takashima et al., 2011). These mice also show impaired cognitive functions, resulting in schizophrenia-like and claustrophobia-like behaviors (Takashima et al., 2011; Voikar et al., 2013). *Lrrtm4*-KO mice also exhibit impaired excitatory synaptic transmission and reduced excitatory synapse density in DG granule neurons, but not in CA1 pyramidal neurons (Siddiqui et al., 2013). Not surprisingly, all four LRRTMs are associated with various neuropsychiatric disorders (de Wit and Ghosh, 2014).

Here, we focus on LRRTM3 to address a subset of key questions left unanswered by prior studies. We found that two different LRRTM3 variants produced by alternative splicing, L3S and L3L, differ with respect to PSD-95 binding, although they exhibit comparable synapse-boosting effects when presented in heterologous synapse-formation assays or overexpressed in cultured hippocampal DG neurons. However, we found that L3S, but not L3L, is required for activity-induced AMPA receptor surface expression in DG neurons. Using *Lrrtm3*-KO mice, we also showed that loss of LRRTM3 led to marked reductions in excitatory synapse density and spontaneous synaptic transmission and excitability in DG granule neurons, but not in CA1 pyramidal neurons. Furthermore, LRRTM3 bound to both glypican-4 (GPC-4) and neurexins in vitro but required only the latter to induce presynaptic differentiation in heterologous synapse-formation assays via distinct alternative splicing-dependent mechanisms. Taken together, these data suggest that LRRTM3 maintains DG excitatory synapse development through both distinct molecular mechanisms and mechanisms shared with other LRRTM family members and that presynaptic neurexins are functionally common ligands for the LRRTM family of synaptic adhesion molecules.

RESULTS

Alternative Splicing Produces LRRTM3 Variants with Both Distinct and Shared Biochemical and Cellular Properties

All LRRTMs have been shown to contain a C terminus that binds to type I PDZ proteins (Laurén et al., 2003; Linhoff et al., 2009), but alternative splicing of *Lrrtm3* and *Lrrtm4* mRNA also produces longer protein variants, LRRTM3L (L3L) and LRRTM4L (L4L), with a unique, presumably non-PDZ-binding C terminus (Figures 1A and S1). The corresponding sequences, encoded by the alternatively spliced 3′-most exon (exon-3), are evolutionarily conserved, suggesting the importance of the intracellular region of these LRRTM variants (Figures 1A and S1). Semiquantitative and qRT-PCR analyses indicated that at postnatal day 14 (P14) in the mouse, *Lrrtm3S* mRNA is expressed almost exclusively in the cerebellum, whereas *Lrrtm3L* shows expression in several brain areas (Figure 1B). In the adult brain, expression of *Lrrtm3S* becomes more widespread, but it is still highest in the cerebellum. The two *Lrrtm4* splice variants show a similar, widespread pattern of expression in several CNS areas at P14, with strongest expression in the cerebral cortex, hippocampus, and olfactory bulb. In the adult brain, the expression pattern is similar, but the level of *Lrrtm4L* expression is reduced (Figure 1B). These RT-PCR results are in general agreement with the pattern of *Lrrtm3 and Lrrtm4* expression reported in a previous in situ hybridization study of adult mouse brain using a probe that detected both mRNA variants (Laurén et al., 2003).

LRRTM1, LRRTM2, and LRRTM4 are localized to the PSD of excitatory synapses (de Wit et al., 2009, 2013; Linhoff et al., 2009; Siddiqui et al., 2013), but the distribution of LRRTM3 has not been investigated. For this purpose, we sought to generate polyclonal antibodies against various immunogenic sequences in either L3L or L3S (data not shown) and were able to successfully develop an antibody against a C-terminal sequence of L3L (Figure S2A). This antibody (JK092) was specific for L3L (did not cross-react with L3S) and produced a single immunoreactive band of ~75 kDa in western blots of the synaptosomal fraction of adult rat brains (Figure S2B). The expression of L3L gradually increased during postnatal brain development (Figure S2C). Moreover, L3L proteins were detected in various subcellular fractions, including crude synaptosomes (P2) and synaptic membranes (LP1) (Figure S2D). Notably, L3L was enriched in detergent-resistant PSD fractions (Figure S2E). These data indicate that LRRTM3 (at least L3L) is associated with excitatory synaptic membranes. In accord with biochemical data, confocal microscopy revealed that L3L immunoreactivity was closely associated with the excitatory marker proteins VGLUT1 and PSD-95, but not with the inhibitory marker proteins GAD67 and gephyrin in cultured hippocampal neurons (Figures S2F–S2J). L3L immunoreactivity was also prominent outside VGLUT1- or PSD-95-positive excitatory synaptic sites, consistent with its widespread distribution in various subcellular fractions (see Figure S2D). To corroborate these observations, we expressed monomeric Venus (mVenus) fluorescent protein fused to L3L (L3L-mVenus) in cultured hippocampal neurons and immunostained them for VGLUT1 and PSD-95 (Figure S2K). mVenus immunofluorescence in L3L-mVenus-expressing neurons was

clustered at excitatory synapse sites (55% ± 5% and 49% ± 6% of L3L-mVenus-positive puncta matches with PSD-95 and VGLUT1, respectively), suggesting that endogenous L3L proteins, similar to L3S, localize to excitatory synapses (Minatohara et al., 2015).

Next, we performed in situ hybridization analyses of mouse brains in various developmental stages using individual isoform-specific probes (Figure 1C). We found that both long and short isoforms of LRRTM3 and LRRTM4 showed widespread expression, including the DG region of the hippocampus, cerebellum, cerebral cortex, and olfactory bulb (Figure 1C). Notably, we found that both *Lrrtm3L* and *Lrrtm3S* mRNAs are expressed in the DG of the hippocampus of adult mouse brains, although they showed distinct expression patterns throughout mouse brain development (Figure 1C). In contrast, the distribution patterns of *Lrrtm4S* and *Lrrtm4L* mRNAs were similar and were not significantly changed in developing and adult brains (Figure 1C). As expected, we confirmed that L3S and L4S, but not L3L or L4L, interacted with PSD-95, as determined by coimmunoprecipitation assays in HEK293T cells and coclustering assays in COS-7 cells (Figures 1D and 1E). Collectively, these data indicate that distribution patterns in developing and adult mouse brains and PSD-95-binding properties of alternative splice variants of LRRTM3 are distinct but share the same excitatory synapse localization.

Overexpression of LRRTM3 Increases Excitatory Synapse Numbers in DG Granule Neurons

LRRTM3 was previously reported to exhibit the lowest synaptogenic activity among the four LRRTMs in heterologous synapse-formation assays (de Wit et al., 2009; Linhoff et al., 2009). However, we found that the newly engineered L3S and L3L constructs displayed a strong ability comparable to that of LRRTM2 (L2) and LRRTM4 (L4S and L4L) to trigger presynaptic differentiation in cultured hippocampal neurons, suggesting that LRRTM3 also possesses potent synaptogenic activity (Figures 1F and 1G).

Next, we examined whether LRRTM3 exhibits synapse-promoting activities by transfecting hippocampal neurons at 10 days in vitro (DIV10) with mVenus-fused L3L or L3S and immunostaining them at DIV14 for excitatory synaptic markers (VGLUT1 and Shank) and for inhibitory synaptic markers (GAD67 and gephyrin) (Figures 1H, 1I, and S3). Because *Lrrtm3* mRNAs are specifically expressed in the DG and not in other subfields of the hippocampus (Figure 1C; Laurén et al., 2003), we classified the transfected neurons based on their immunoreactivity for Prox1, a DG granule neuron-specific marker, and CTIP2, a CA1/DG neuron marker, and analyzed them separately (Figures 1H, 1I, and S3). We found that both L3S and L3L exhibited excitatory, but not inhibitory, synapse-promoting activities in cultured hippocampal DG neurons (Figures 1H and 1I). The synapse-promoting activity of L3S and L3L were restricted to Prox1-positive DG neurons (Figures 1H, 1I, and S3). In addition, overexpression of L3L increased excitatory postsynapse specialization (labeled by Shank), but not inhibitory postsynapse specialization (labeled by gephyrin) (Figure S3). Taken together, these results suggest that both LRRTM3 splice variants are synaptogenic, inducing presynaptic differentiation and increasing excitatory synapse number.

LRRTM3 Knockdown Reduces Excitatory Synapse Numbers in DG Granule Neurons

To examine whether endogenous LRRTM3 is required for excitatory synapse development in DG granule neurons, we first designed small hairpin RNAs (shRNAs) that targeted *Lrrtm3* or *Lrrtm4* mRNA (Figures S4A and S4B). To test their effectiveness, we expressed shRNAs in cultured mouse cortical neurons using lentiviruses and quantified endogenous target mRNA levels by qRT-PCR (Figure S4B). These experiments identified shRNAs that suppressed expression of endogenous mRNAs for *Lrrtm3* (J16) and *Lrrtm4* (J30) by ~80% and 90%, respectively (Figure S4B). We then investigated whether single KD of LRRTM3 or LRRTM4 altered synapse numbers in cultured DG neurons (Figure 2). To accomplish this, we transfected cultured DG neurons at DIV8 with vectors that express only EGFP (control) or coexpress EGFP with shRNAs against *Lrrtm3* (L3 KD) or *Lrrtm4* (L4 KD). We then immunostained the transfected neurons for VGLUT1 or GAD67 at DIV14 and quantified the density of excitatory and inhibitory synapses on dendrites of the transfected neurons (Figures 2A–2D). We found that the synapse loss induced by L3 or L4 KD was specific for excitatory synapses and not for inhibitory synapses (Figures 2A–2D). Strikingly, double KD of LRRTM3 and LRRTM4 (L3/L4 DKD) did not further decrease the excitatory synapse numbers than KD of either protein alone, suggesting that both LRRTM3 and LRRTM4 may share common pathways in maintenance of excitatory synapse structure at DG neurons (Figures 2A–2D). More importantly, coexpression of an shRNA-resistant form of L3S or L3L (i.e., rescue vectors) completely eliminated the deficits in excitatory synapse density observed with L3 KD (Figures 2A–2D), confirming that the observed phenotypes are not attributable to off-target effects. Collectively, these data complement the results obtained with gain-of-function experiments (described above).

LRRTM3 Controls Synaptic-Activity-Induced AMPA Receptor Surface Expression in an Alternative-Splicing-Dependent Manner

It was previously reported that LRRTM2 and LRRTM4 associate with AMPA receptors (Aoto et al., 2013; de Wit et al., 2009; Schwenk et al., 2012; Siddiqui et al., 2013; Soler-Llavina et al., 2013). Specifically, LRRTM2 was shown to directly interact with the GluA1 subunit of AMPA receptors, and both LRRTM2 and LRRTM4 were found to promote synaptic NMDA receptor activity-dependent stabilization of the AMPA receptor population, contributing to the regulation of extrasynaptic surface AMPA receptor trafficking or endocytosis (Siddiqui et al., 2013; Soler-Llavina et al., 2013). To determine whether LRRTM3 is also involved in similar cell-biological events in DG neurons, we transfected cultured DG neurons at DIV8 with vectors that express EGFP (control) or sh-LRRTM3 (L3 KD) or coexpress L3 KD and shRNA-resistant LRRTM isoforms (+L3S rescue or +L3L rescue). At DIV14, these neurons were stimulated with cLTP solution (or control solution) for 5 min. Neurons were then fixed and immunostained for surface expression of the GluA1 subunit of AMPA receptors and imaged by confocal microscopy (Figures 3A and 3B). We found that LRRTM3 KD led to a significant reduction in surface AMPA receptors following cLTP (Figures 3A and 3B). Strikingly, this phenotype

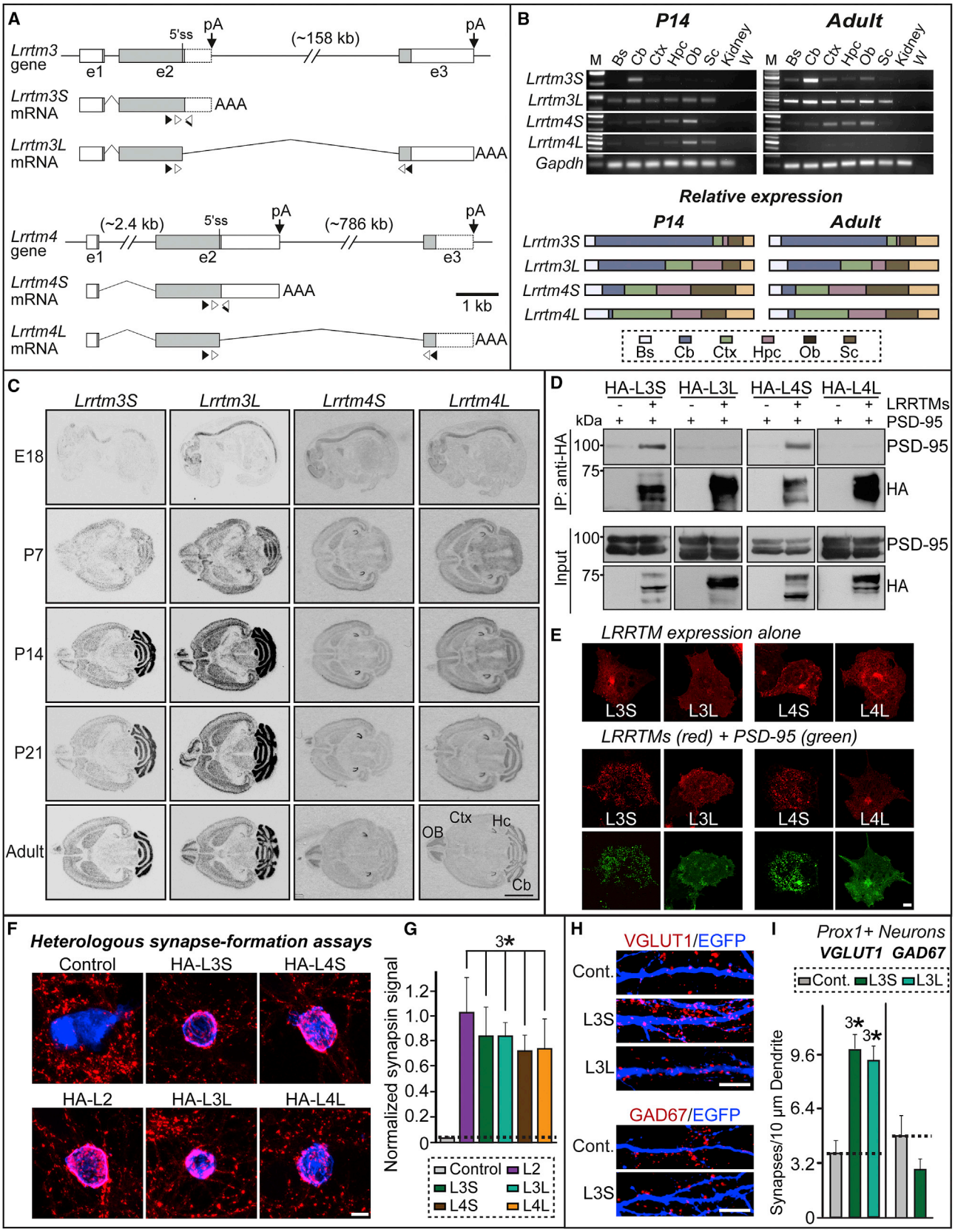

(legend on next page)

was completely reversed by the simultaneous expression of L3S wild-type (WT), but not L3L or the L3S point mutant (L3S VA, an L3S that does not bind PSD-95) (Figures 3A and 3B). These observations were also recapitulated using neurons from Lrrtm3-KO mice (Figures 3C and 3D; see below). Thus, LRRTM3, similar to LRRTM2 and LRRTM4, is required to maintain a subpopulation of AMPA receptors that is responsive to cLTP stimulation. At this point, it is not apparent why the LRRTM3 splice variants show differential behaviors in terms of activity-regulated synaptic insertion of AMPA receptors, but a plausible scenario would be that L3S controls activity-dependent AMPA receptor trafficking through the PSD-95/TARP complex, which is not available for L3L.

Lrrtm3-KO Mice Exhibit Morphological Defects in Excitatory Synapse Development in DG Granule Neurons

To investigate whether LRRTM3 is required for synapse structure and function in vivo, we utilized Lrrtm3-KO mice (Laakso et al., 2012) (see Figures S4C and S4D). We first confirmed that LRRTM3 mRNA transcripts are not detectable by in situ hybridization analyses (Figure 4A). Western blot analyses using an L3L-specific antibody further showed that LRRTM3 protein expression was also completely abolished in these mice (Figure S4D; data not shown). We performed Nissl staining to show the normal gross morphology of Lrrtm3-KO brains (Figure 4B). Expressions of other synaptic proteins were not quantitatively altered at either P14 or P42 in Lrrtm3-KO brains compared with WT brains (Figures 4C, 4D, and S4E).

A quantitative immunofluorescence analysis revealed a significant decrease in the intensity of VGLUT1 puncta in DG molecular layers (MML), but not in the CA1 stratum oriens (oriens), a phenotype similar to that observed in Lrrtm4-KO mice (Figures 4E and 4F; Siddiqui et al., 2013). In contrast, the intensity of GAD67 puncta was unchanged in both DG MML and CA1 oriens (Figures 4E and 4F). We next analyzed dendritic spine density in Golgi-stained brain sections. Spine density on dendrites in DG granule neurons was also significantly reduced in Lrrtm3-KO mice compared with WT littermates (Figures S4F and S4G).

Moreover, electron microscopy analyses showed that the number of dendritic spines (i.e., asymmetric/excitatory synapses) in the DG middle molecular layer (MLL) was modestly, but significantly, decreased at P14 (~20%) and P42 (~15%) in Lrrtm3-KO mice (Figures 5A–5C, S5A, and S5B). This reduction in excitatory synapse density at the ultrastructural level was not observed in the CA1 pyramidal neurons of Lrrtm3-KO mice (Figures 5A–5C). In contrast, the number of GABA-positive presynaptic boutons (i.e., symmetric/inhibitory synapse) in the DG was not reduced in Lrrtm3-KO mice (Figures 5D–5F). The thickness and length of excitatory PSD- or GABA-positive boutons were unchanged by ablation of LRRTM3 protein (Figures 5D–5F). Collectively, these results demonstrate that the loss of LRRTM3 protein decreases the number of excitatory synapses in vivo without altering their gross ultrastructure.

Figure 1. Expression Patterns of Alternative Splice Variants of LRRTM3 and LRRTM4 and Alternative Splicing in LRRTM3 Regulates Interaction with PSD-95, but Not Synapse-Promoting Activities

(A) Structures of mouse *Lrrtm3* and *Lrrtm4* genes, consisting of three coding exons (e1–e3), and transcripts encoding the long and short isoforms, resulting from alternative splicing and polyadenylation. Exons are shown as boxes. Coding and non-coding exonic regions are in gray and white, respectively. Splicing is indicated by an angled line. The sizes of long introns are shown in parenthesis. The primers used for quantitative and semiquantitative RT-PCR are marked by white and black arrowheads, respectively. The transcripts correspond to the following ENSEMBL IDs with the highest Transcript Support Level: ENSMUST00000105439 (*Lrrtm3L*), ENSMUST00000136421 (*Lrrtm4S*), and ENSMUST00000147663 (*Lrrtm4L*). The length of the 3′ UTR in *Lrrtm3S* (and in *Lrrtm4L*) transcripts is predicted.

(B) Semiquantitative analysis of *Lrrtm3* and *Lrrtm4* expression by RT-PCR in P14 and adult mice. Representative gel images (top) show expression of *Lrrtm3S* (*L3S*), *Lrrtm3L* (*L3L*), *Lrrtm4S* (*L4S*), *Lrrtm4L* (*L4L*) and control *Gapdh* mRNAs in different brain regions and kidney from three independent experiments. Summary histograms of qRT-PCR (bottom) show *Lrrtm3* and *Lrrtm4* mRNA expression in different brain regions of P14 and adult mice (n = 4 mice for each tissue). Bs, brain stem; Cb, cerebellum; Ctx, cortex; Hpc, hippocampus; Ob, olfactory bulb; Sc, spinal cord; and W, water.

(C) Expression of *Lrrtm3* and *Lrrtm4* mRNAs in developing and adult mouse brains. Sections from embryonic day 18 (E18), P7, P14, P21, and adult (6-week-old) mouse brains were probed with L3L-, L3S-, L4L, and L4S-specific cRNAs. Cb, cerebellum; Ctx, cerebral cortex; Hc, hippocampus; and OB, olfactory bulb. Scale bar represents 5 mm (applies to all images).

(D) Coimmunoprecipitation experiment demonstrating that L3S and L4S, but not L3L or L4L, interact with PSD-95. Untagged PSD-95 was transfected alone or together with hemagglutinin (HA)-tagged LRRTMs, as indicated, into HEK293T cells, and coimmunoprecipitation of PSD-95 with LRRTMs was assayed by immunoblotting. A representative immunoblot, visualized using enhanced chemiluminescence, is shown.

(E) Coclustering experiment performed in COS-7 cells demonstrating that L3S and L4S, but not L3L or L4L, interact with PSD-95. COS-7 cells were transfected with HA-tagged LRRTMs (red), alone or together with EGFP-PSD-95 (green), and visualized by double immunofluorescence staining with anti-EGFP and anti-HA antibodies.

(F and G) Representative images of heterologous synapse-formation assays (F) and summary graphs (G). Hippocampal neurons were cocultured for 2 days with HEK293T cells expressing EGFP alone (control), HA-tagged LRRTM2 (L2), HA-tagged LRRTM3L (L3L), HA-tagged LRRTM3S (L3S), HA-tagged LRRTM4L (L4L), or HA-tagged LRRTM4S (L4S). Cocultured neurons were immunostained with antibodies to EGFP/HA (blue) and the presynaptic marker synapsin I (red). Heterologous synapse-formation activity of LRRTMs, quantified as the ratio of synapsin staining to HA fluorescence. Coincident blue and red signals are shown in violet. Data shown are means ± SEMs; statistical significance was assessed by comparing the various conditions to controls using Student's t test (n denotes the number of HEK293T cells analyzed as follows: Control, n = 15; HA-L3S, n = 12; HA-L3L, n = 14; HA-L4S, n = 16; HA-L4L, n = 18; and HA-L2, n = 12). Scale bar represents 25 μm (applies to all images).

(H and I) Representative images (H) of Prox1-positive cultured hippocampal DG neurons transfected at DIV10 with EGFP alone (Control), an LRRTM3S mVenus-fusion protein (L3S-mVenus), or an LRRTM3L mVenus-fusion protein (L3L-mVenus). Cultures were analyzed at DIV14 by double immunofluorescence with antibodies to EGFP (blue) and VGLUT1 (excitatory presynaptic marker) or GAD67 (inhibitory presynaptic marker; red). Scale bar represents 5 μm (applies to all images). Effects of LRRTM3 on synapse density were quantified (I). All data shown in (G) and (I) are means ± SEMs; statistical significance was assessed by comparing the various conditions to controls using Student's t test (^{3}*$p < 0.001$; n denotes the number of neurons analyzed as follows: Cont./VGLUT1, n = 12; L3S/VGLUT1, n = 18; L3L/VGLUT1, n = 13; Cont./GAD67, n = 12; and L3S/GAD67, n = 13).

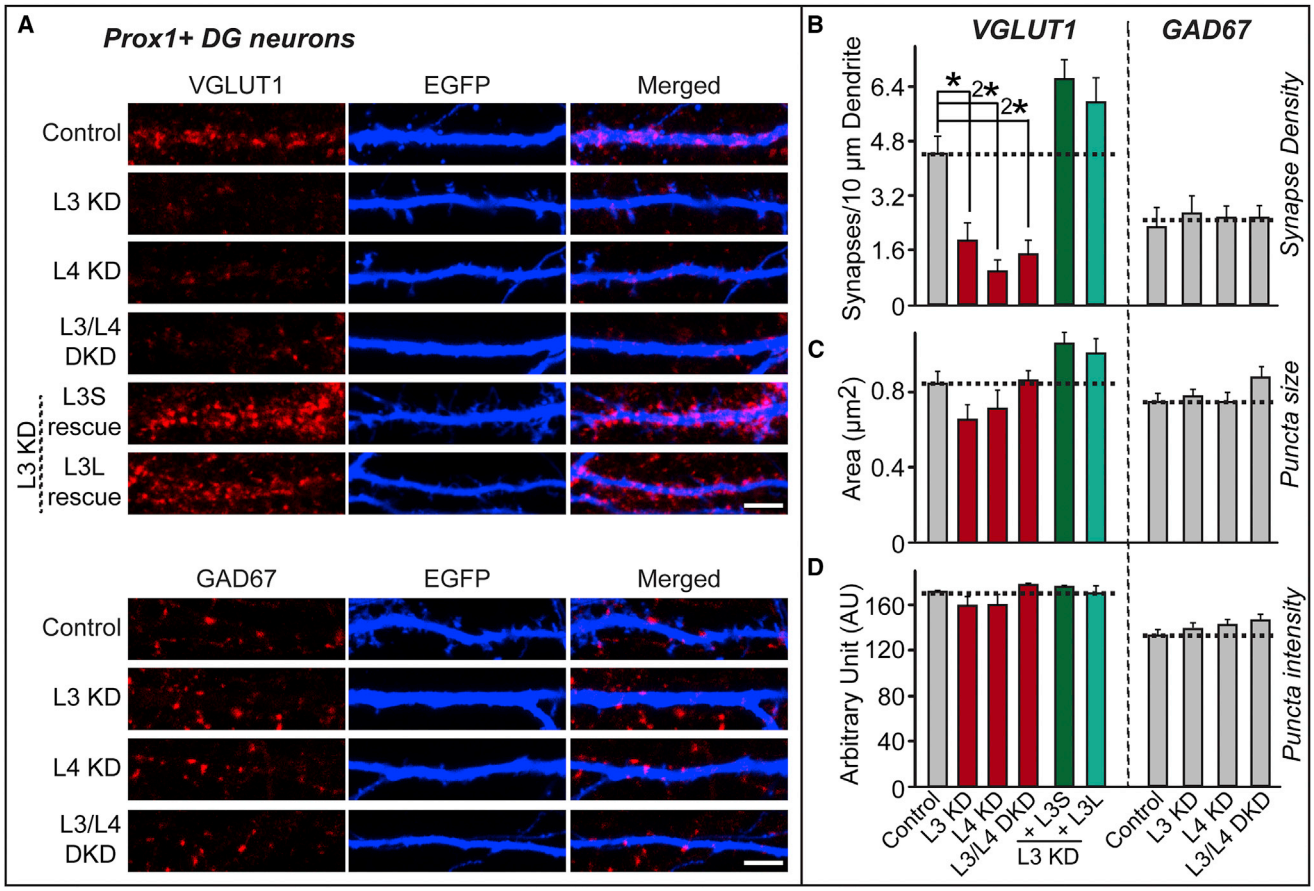

Figure 2. Knockdown of LRRTM3 Reduces Excitatory Synapse Numbers in DG Granule Neurons

(A) Representative images of cultured hippocampal DG neurons transfected at DIV8 with a lentiviral vector expressing EGFP alone (Control), LRRTM3 knockdown (L3 KD; with/without L3S or L3L rescue vectors), LRRTM4 KD (L4 KD) or LRRTM3/4 double KD (L3/L4 DKD), and analyzed by double immunofluorescence with antibodies to EGFP (green) and VGLUT1 or GAD67 (red) at DIV14. Scale bar represents 5 μm (applies to all images).

(B–D) Summary graphs of the effects of single or double KD of LRRTM3 and/or LRRTM4 on marker puncta density (B); quantified using VGLUT1 or GAD67 immunoreactivity), puncta size (C) and puncta intensity (D), and phenotypic restoration by LRRTM3S (L3S rescue), but not by LRRTM3L (L3L rescue). L3 and L4 denote LRRTM3 and LRRTM4. Data shown are means ± SEMs from three independent culture experiments; statistical significance was assessed by comparing the various conditions to controls using ANOVA with Tukey's test (*$p < 0.05$ and $^{2*}p < 0.01$; n denotes the number of neurons analyzed as follows: Control/VGLUT1, n = 12; L3 KD/VGLUT1, n = 12; L4 KD/VGLUT1, n = 12; L3/L4 DKD/VGLUT1, n = 12; L3S rescue/VGLUT1, n = 14; L3L rescue/VGLUT1, n = 12; Control/GAD67, n = 13; L3 KD/GAD67, n = 12; L4 KD/GAD67, n = 12; and L3/L4 DKD/GAD67, n = 12).

Excitatory Synaptic Transmission Is Specifically Impaired in DG Granule Neurons of Lrrtm3-KO Mice

To determine whether excitatory synaptic function is changed as a result of genetic perturbation of LRRTM3, we performed whole-cell recordings from DG granule cells in hippocampal slices from WT and Lrrtm3-KO mice (Figure 6). We found that the amplitude of miniature excitatory postsynaptic currents (mEPSCs) was markedly reduced in LRRTM3-deficient neurons (Figures 6A–6C). The amplitude of spontaneous excitatory events (sEPSCs) was reduced to the same extent in Lrrtm3-KO neurons (Figures 6D and 6E). Strikingly, the frequency of mEPSCs was significantly increased in neurons from Lrrtm3-KO mice compared with those from WT mice, whereas the frequency of sEPSCs was not altered (Figures 6A–6E). No changes were observed in the frequency or amplitude of miniature inhibitory postsynaptic currents (mIPSCs) (Figures 6D and 6F).

Next, to examine whether the intrinsic excitability of DG granule neurons is affected by LRRTM3 loss, we determined the firing rate of DG granule neurons from Lrrtm3-KO mice using the current-clamp configuration of the patch-clamp technique (Figures 6G and 6H). DG granule cells were injected with 500-ms current steps, ranging from −50 to 250 pA in 50-pA increments. The firing rate of DG granule neurons in LRRTM3-KO slices was lower than that of neurons in WT slices (Figures 6G and 6H). In contrast, recordings from CA1 pyramidal neurons revealed no differences in the firing rates of WT and Lrrtm3-KO neurons (Figures 6G and 6H) and no changes in intrinsic membrane properties (Table S2). These results indicate that the deficits in excitatory synaptic transmission observed in LRRTM3-KO neurons are accompanied by reduced excitability in DG granule cells. We also found that *Lrrtm3* ablation decreased paired-pulse ratios, a measure of presynaptic neurotransmitter

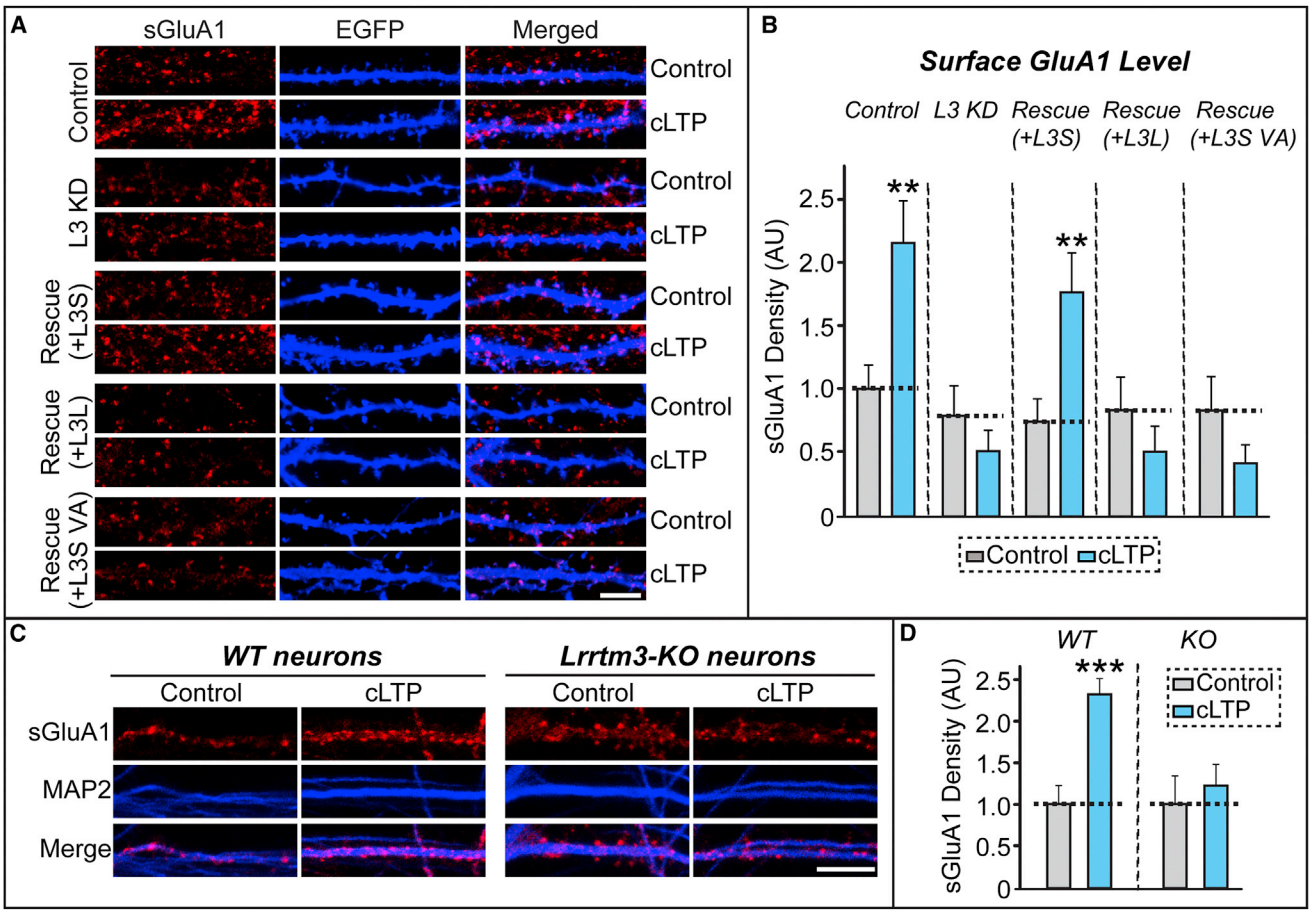

Figure 3. LRRTM3 Controls cLTP-induced Surface AMPA Receptor Expression in DG Granule Neurons in an Alternative Splicing-Dependent Manner

(A) Representative images of cultured hippocampal DG neurons transfected at DIV8 with a lentiviral vector expressing EGFP alone (Control) or LRRTM3 KD (L3 KD; with/without L3S or L3L rescue vectors), and analyzed by triple immunofluorescence with antibodies to Prox1 (not shown), EGFP (blue), and AMPA receptor subunit GluA1 (red) 20 min after treatment with control (Control) or glycine-containing solution (+ cLTP) at DIV14. Scale bar represents 5 μm (applies to all images).

(B) Summary graphs showing surface GluA1 puncta intensity in various experimental culture sets, as indicated. Data shown are means ± SEMs from three independent culture experiments; statistical significance was assessed by comparing the various conditions to controls using ANOVA with Tukey's test (**$p < 0.01$; n denotes the number of neurons analyzed as follows: Control/Control, n = 14; Control/L3 KD, n = 14; Control/L3 KD (+L3S WT rescue), n = 14; Control/L3 KD (+L3S VA rescue), n = 14; Control/L3 KD (+L3L rescue), n = 14; cLTP /Control, n = 14; cLTP /L3 KD, n = 14; cLTP /L3 KD (+L3S WT rescue), n = 14; cLTP/L3 KD (+L3S VA rescue), n = 14; and cLTP/L3 KD (+L3L rescue), n = 14).

(C) A chemical LTP (cLTP) containing glycine led to a selective increase in surface GluA1 in WT, but not LRRTM3-*KO*, DG granule neurons identified by Prox1 immunoreactivity. Scale bar represents 5 μm (applies to all images).

(D) Quantification of integrated intensity of surface GluA1 normalized to control condition. All data are expressed as means ± SEMs; statistical significance was assessed in comparison to controls using Student's t test (***$p < 0.001$; n denotes the number of neurons analyzed as follows: Control/WT, n = 14; cLTP/WT, n = 14; Control/KO, n = 14; and cLTP/KO, n = 14).

release probability, at an interstimulus interval of 20 ms (Figures 6I and 6J). In addition, input-output curves of excitatory synaptic transmission at perforant pathway (PP) to DG granule neurons, measured by patch-clamp recordings, revealed a small decrease in evoked excitatory synaptic transmission in Lrrtm3-KO mice compared with WT mice, but the maximal response was comparable (Figures S6A and S6B). Furthermore, a 20-Hz stimulus led to much faster depression of evoked EPSC amplitude in Lrrtm3-KO mice (Figures S6C and S6D). These results suggest that loss of LRRTM3 results in increased neurotransmitter release, leading to a slower recovery of the releasable vesicle pool. Finally, we examined whether long-term synaptic plasticity is altered in Lrrtm3-KO mice (Figure S6E). Long-term potentiation (LTP) was induced via high-frequency stimulation (HFS) of PP-to-DG synapses. Our data showed that deletion of LRRTM3 tends to decrease LTP by 15% in PP-to-DG synapses (but did not reach a statistically significant decrease in LTP) (Figure S6E). Collectively, our electrophysiology data demonstrate that LRRTM3 is postsynaptically required for excitatory synaptic transmission in DG granule neurons.

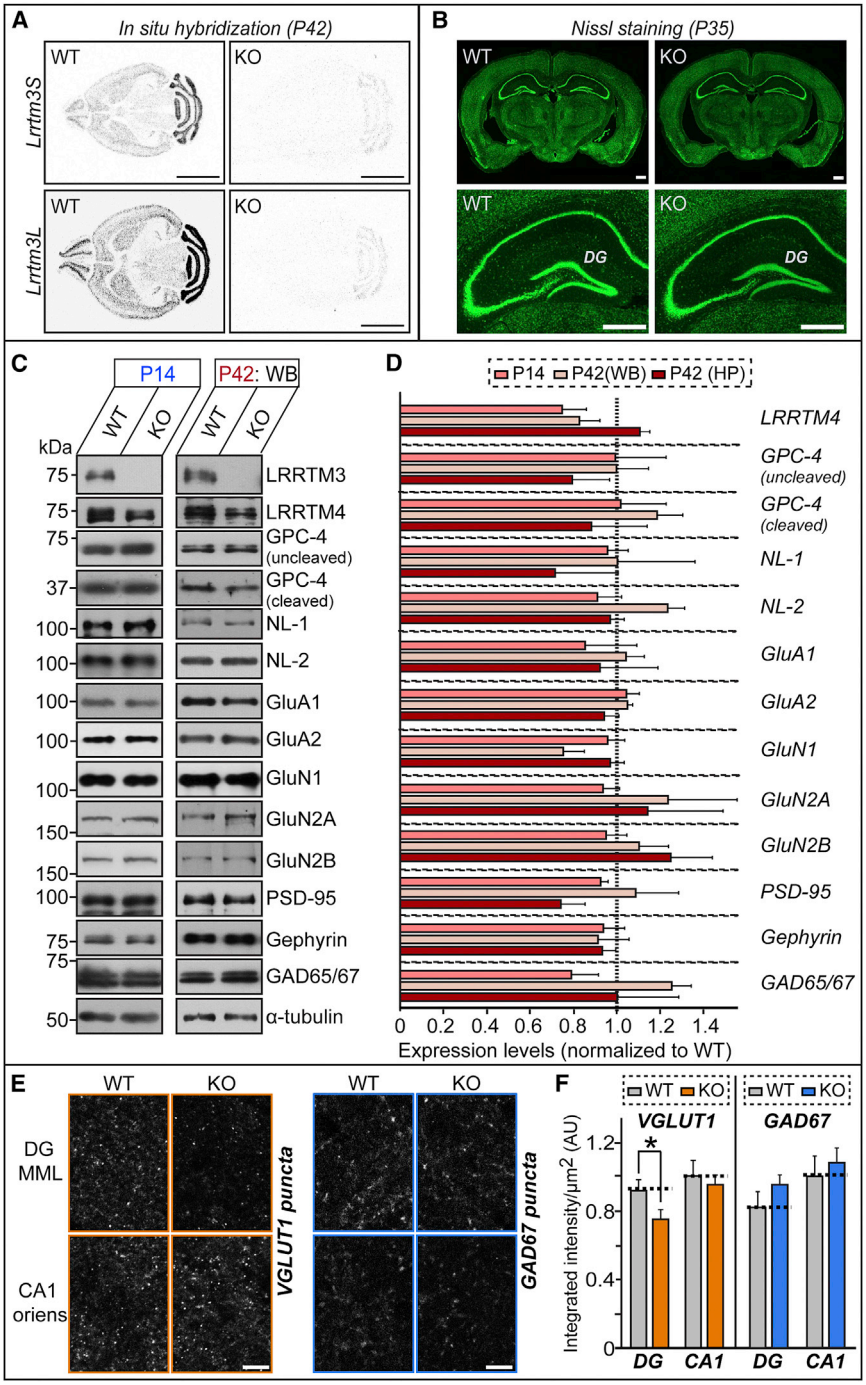

Figure 4. Excitatory Synapse Development is Impaired in the DG of Lrrtm3-*KO* Mice

(A) Validation of the lack of *Lrrtm3* mRNAs in adult (P42) WT or Lrrtm3-KO brains by in situ hybridization. Three different cRNAs were used: *L3S* to detect *LRRTM3S*, but not *LRRTM3L*; and *L3L* to detect *LRRTM3L*, but not *LRRTM3S*. Scale bar represents 5 mm (applies to all images).

(B) Normal gross morphology of the Lrrtm3-KO brain at P35. Hippocampal DG morphology is highlighted for comparison to normal DG layered structures of the age-matched WT brain. Scale bar represents 500 μm (applies to all images).

(C and D) Representative immunoblots (C) and summary graphs of synaptic protein levels (D) in crude synaptosomal fractions of P14 and P42 WT and Lrrtm3-KO brains (3-5 pairs) analyzed by semiquantitative immunoblotting. Hippocampal fractions (HP) from P42 WT and Lrrtm3-KO mice were further dissected and analyzed in parallel. Statistical significance was assessed using ANOVA with Tukey's test. For additional immunoblot images, see Figure S4E.

(E) Confocal images revealed a reduction in VGLUT1 puncta intensity in the DG molecular layer of Lrrtm3-KO mice at P42 compared with age-matched WT mice but not in the CA1 stratum oriens. No difference was observed in GAD67 puncta intensity. Scale bar represents 10 μm (applies to all images).

(F) Quantification of VGLUT1 and GAD67 puncta intensity per tissue area. Data shown are means ± SEMs from three independent culture experiments; statistical significance was assessed by comparing the various conditions to controls using ANOVA with Tukey's test (*$p < 0.05$; $n = 3$ mice for all conditions). For Golgi-COX stained images, see Figures S4F and S4G.

LRRTM3 Requires Specific Neurexin Splice Variants for Presynaptic Differentiation

LRRTM3 regulates the maintenance of surface AMPA receptors in a synaptic activity- and alternative-splicing-dependent manner (Figure 3). However, it remains to be determined how LRRTM3 performs its synapse-promoting functions. Specifically, the extracellular ligands of LRRTM3 have not been clearly defined, in part because LRRTM3 was previously reported to exert marginal synaptogenic activity (de Wit et al., 2009; Linhoff et al., 2009). Nonetheless, GPC-4 and/or neurexins have been postulated as candidate ligands for LRRTM3 (de Wit et al., 2013; Ko et al., 2009; but see Siddiqui et al., 2013). We first performed cell surface-binding assays using recombinant immunoglobulin (Ig)-fusion proteins of GPC-4 (Ig-GPC-4) and HEK293T cells expressing LRRTM3-mVenus (Figure S7A). We found that LRRTM3 avidly bound to GPC-4 (Figure S7A), similar to LRRTM4 (de Wit et al., 2013; Ko et al., 2015b). Pull-down assays with Ig-neurexin-1β fusion proteins lacking an insert at splice site 4 (SS4) showed that LRRTM3 also interacted with neurexin-1β, at least in vitro (Figure S7B; Ko et al., 2009). To address previously unresolved issues surrounding LRRTMs, we performed an extensive series of heterologous synapse-formation assays (Figure 7). First, we asked whether presynaptic neurexins or glypicans are required for the synaptogenic activity of LRRTM3. In the case of glypicans, we generated

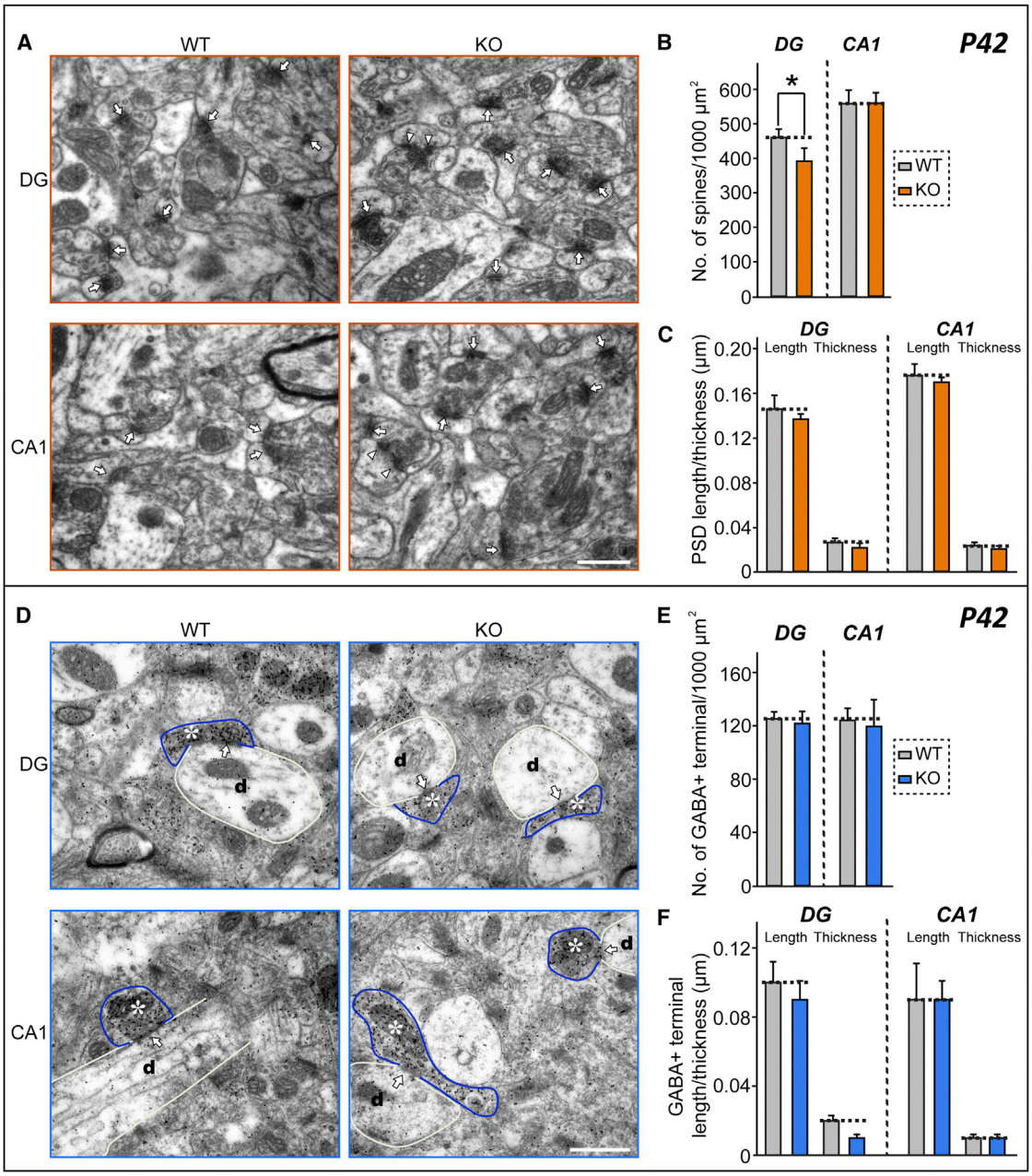

Figure 5. Lrrtm3-*KO* Mice Exhibit Decreased Excitatory Synapse Density in the DG, but Not the CA1 Region, of the Hippocampus

(A–C) Representative electron microscopy images (A) and summary graphs of excitatory synapse density (B) and PSD length and thickness (C) of the DG molecular layer and CA1 stratum radiatum from WT and Lrrtm3-KO mice (KO) at P42. Data shown are means ± SEMs (WT_{DG}, n = 60 images, 392 synapses, 3 male littermates; KO_{DG}, n = 60 images, 347 synapses, 3 males; WT_{CA1}, n = 60 images, 472 synapses, 3 male littermates; KO_{CA1}, n = 60 images, 470 synapses, 3 males). White arrows indicate the PSD in dendritic spines of excitatory synapses, and arrowheads indicate perforated synapses. Statistical significance was assessed using Student's t test (*$p < 0.05$). Scale bar represents 500 nm (applies to all images).

(D–F) Representative electron microscopy images (D) and summary graphs of inhibitory synapse density (E) and GABA-positive terminal length and thickness (F) of the DG molecular layer and CA1 stratum radiatum from WT and Lrrtm3-KO mice (KO) at P42. Data shown are means ± SEMs (WT_{DG}, n = 60 images, 109 synapses, 3 male littermates; KO_{DG}, n = 60 images, 106 synapses, 3 males; WT_{CA1}, n = 60 images, 108 synapses, 3 male littermates; KO_{CA1}, n = 60 images, 104 synapses, 3 males). White arrows indicate synapse structure, asterisks indicate GABA-positive presynaptic terminals, and "d" denotes dendrites. Statistical significance was assessed using Student's t test. Scale bar represents 500 nm (applies to all images).

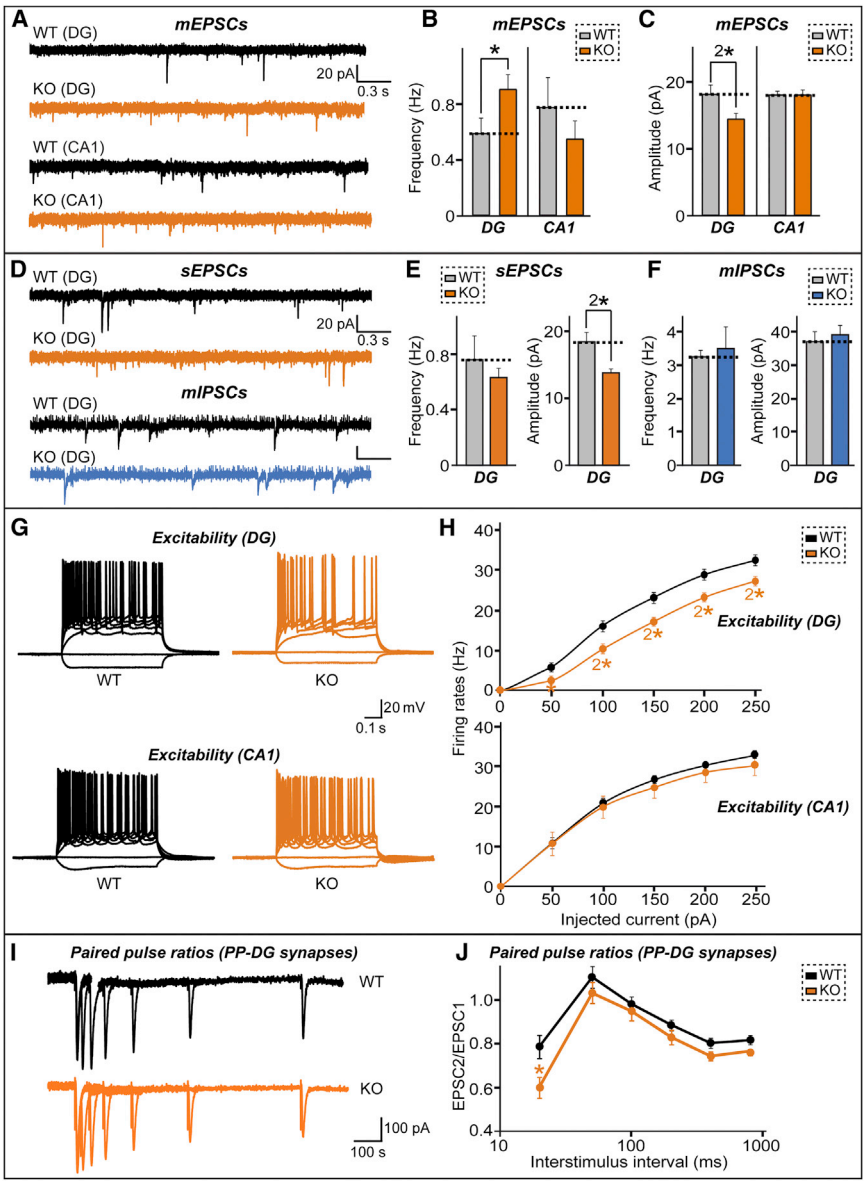

Figure 6. Lrrtm3-*KO* Mice Display Impaired Excitatory Synaptic Transmission in DG Granule Neurons

(A–C) Representative traces (A) and summary graphs (B) and (C) of mEPSCs recorded from DG and CA1 regions of the hippocampus in WT (gray) or Lrrtm3-KO mice (orange). Graphs show means ± SEM (*$p < 0.05$ and $^{2*}p < 0.01$, Mann-Whitney U test; n denotes the total number of neurons analyzed as follows: mEPSCs/WT_{DG}, n = 14 cells/5 mice; mEPSCs/KO_{DG}, n = 14 cells/3 mice; mEPSCs/WT_{CA1}, n = 15 cells/4 mice; and mEPSCs/KO_{CA1}, n = 17 cells/3 mice).

(D–F) Representative traces (D) and summary graphs of sEPSCs (orange) (E) or mIPSCs (blue) (F) recorded from DG and CA1 regions of hippocampus in WT (gray) and Lrrtm3-KO mice. Graphs show means ± SEM (*$p < 0.05$, Mann-Whitney *U* test; sEPSCs/WT_{DG}, n = 12 cells/4 mice; sEPSCs/KO_{DG}, n = 9 cells/2 mice; mIPSCs/WT_{DG}, n = 17 cells/3 mice; and mIPSCs/KO_{DG}, n = 13 cells/2 mice).

(G and H) Representative traces (G) and summary graphs (H) of intrinsic excitability measured as firing rates in response to step depolarizing currents (duration 500 ms) in DG (top) and CA1 (bottom) slices from WT (black) and Lrrtm3-KO mice (orange). Individual points represent means ± SEM (*$p < 0.05$ and $^{2*}p < 0.01$, Mann-Whitney U test; WT_{DG}, n = 16 cells/3 mice; KO_{CA1}, n = 13 cells/3 mice; WT_{CA1}, n = 18 cells/8 mice; and KO_{CA1}, n = 11 cells/5 mice).

(I and J) Representative traces (I) and summary graphs (J) of paired-pulse ratios of AMPA receptor-EPSCs recorded in the perforant pathway to granule cell synapses (PP-DG) from WT (black) and Lrrtm3-KO (orange) mice. Individual points represent means ± SEM (*$p < 0.05$, Mann-Whitney *U* test; WT, n = 15 cells/3 mice and KO, n = 18 cells/4 mice). Note that the paired-pulse ratio in Lrrtm3-KO mice is significantly decreased at an interstimulus interval of 20 ms.

a lentiviral shRNA vector (sh-GPC-1/2/4) that knocks down GPC-1, GPC-2, and GPC-4, all of which (among the six GPCs) are strongly expressed in the hippocampus (Ko et al., 2015b). In addition to this vector, we used previously characterized lentiviral shRNAs against neurexins (sh-Nrx1/2/3) or PTPσ (sh-PTPσ) (Ko et al., 2015b; Um et al., 2014b; Yim et al., 2013). Neurexin triple KD (sh-Nrx1/2/3) drastically reduced the synaptogenic activity of all LRRTMs examined, whereas GPC triple KD (sh-GPC-1/2/4) significantly reduced the synaptogenic activity of only LRRTM4 (Figures 7A and 7B). PTPσ KD (sh-PTPσ) decreased only LRRTM4 activity, consistent with our previous report that LRRTM4 activity is partially mediated by the GPC-4/PTPσ complex (Ko et al., 2015b).

The requirement of presynaptic neurexins for synaptogenic activity was independently investigated in independent heterologous synapse-formation assays using the LRRTM point mutants (designated LRRTM2-EX^{AA}, LRRTM3-EX^{AA}, and LRRTM4-EX^{AA}; Figures 7C and S7C–S7E). The mutated LRRTM residues are all conserved and predicted to abolish neurexin binding (Figure S7C; Siddiqui et al., 2010). Indeed, all LRRTM mutations markedly decreased the synaptogenic activities of individual LRRTMs (Figures 7C and S7D). Lastly, we tested whether a subset of neurexin splice variants are required for LRRTM3 activity. We found that Nrx1β-1 (Nrx1β variant lacking an insert at splice site #SS4), but not Nrx1β-3 (Nrx1β variant containing an insert at #SS4), reversed the deficit in the synapse-formation activity of LRRTM3 observed in neurexin-deficient neurons (Figures 7D and 7E). Intriguingly, both Nrx1β-1 and Nrx1β-3 were equally capable of restoring the deficit in the synapse-formation activity of LRRTM4, consistent with a previous report that LRRTM4

interacts with Nrx1β independent of its alternative splicing status at #SS4 (Figures 7D and 7E; de Wit et al., 2013). Consistent with this interpretation, both Ig-Nrx1β-1 and Ig-Nrx1β-3 pulled down LRRTM4, whereas only Ig-Nrx1β-1 avidly bound to LRRTM3 (Figure S7B). Taken together, these data unequivocally reinforce the conclusion that LRRTM3 primarily mediates its synaptogenic activity through presynaptic neurexins in an alternative splicing-dependent manner.

DISCUSSION

In our current investigation of LRRTM3, we asked whether the PSD-95-binding property of LRRTM3 has any physiological significance and whether presynaptic neurexins are universally required for LRRTM proteins. Most importantly, given the clinical implications of LRRTM3 in autism spectrum disorders (ASDs) and strong expression pattern in the DG—features shared with LRRTM4—we asked how LRRTM3 contributes to specification of excitatory synapse development, at least in the DG, with the goal of shedding light on pathophysiological mechanisms underlying the associated brain disorders. We report five key observations:

1. Both *Lrrtm3* and *Lrrtm4* genes produce (by alternative splicing) two protein variants with different (short or long) C termini, of which only the short variants interact with PSD-95. (Similar alternative splicing events do not exist for *Lrrtm1* or *Lrrtm2*.) This suggests that LRRTM3 and LRRTM4 function may be controlled by as yet unknown but likely region-specific spliceosomal machinery. The expression of LRRTM3/4 splice variants that do not bind to PSD-95 (i.e., L3L and L4L) is also developmentally regulated and shows distribution patterns distinct from those of PSD-95-interacting splice variants (Figures 1B and 1C). However, L3L, similar to L3S, is targeted to excitatory synapse sites in cultured hippocampal neurons (Figure S2K). These data argue that PSD-95 interaction per se does not orchestrate all the synaptic functions mediated by synaptic adhesion molecules. Indeed, even in the case of LRRTM2, excitatory synapse targeting does not rely on PSD-95 interactions (Linhoff et al., 2009; Mintohara et al., 2015); a similar independence of PSD-95 interaction has also been reported for neuroligin-1 (Dresbach et al., 2004). In contrast, netrin-G ligand-2 (NGL-2) requires interaction with PSD-95 for its excitatory synapse targeting (Kim et al., 2006).
2. Overexpression of either LRRTM3 splice variant increased excitatory synapse numbers in DG granule neurons (Figures 1H and 1I), similar to the actions of other LRRTMs in facilitating excitatory synapse development. Conversely, LRRTM3 KD induced a loss of excitatory synapses in DG granule neurons (Figure 2). Re-expression of either LRRTM3 splice variant completely reversed the excitatory synapse reduction caused by LRRTM3 KD (Figure 2), suggesting that the intact extracellular sequences of LRRTM3 are sufficient to promote excitatory synapse development, a feature reminiscent of NL-1 and LRRTM2 (Ko et al., 2011). Notably, double KD of LRRTM3 and LRRTM4 did not further decrease the excitatory synapse loss beyond that induced by either LRRTM3 KD or LRRTM4 KD, suggesting that these two proteins share similar pathways in organizing excitatory synapse development in DG granule neurons, an action dissimilar to that of LRRTM1 and LRRTM2 at CA1 pyramidal neurons (Ko et al., 2011; Soler-Llavina et al., 2011).
3. Most importantly, both LRRTM3 splice variants perform distinct functions in activity-dependent surface expression of AMPA receptors in DG granule neurons (Figure 3). LRRTM2 directly associates with AMPA receptor subunits and is specifically required for maintenance of newly delivered AMPA receptors after cLTP induction; it also controls AMPA receptor trafficking in concert with presynaptic neurexin-3 (Aoto et al., 2013; Soler-Llavina et al., 2013). Like LRRTM2, LRRTM4 forms physical complexes with AMPA receptors and similarly acts to increase surface GluA1 levels after cLTP (Schwenk et al., 2012; Siddiqui et al., 2013). We demonstrated in the current study that KO or KD of LRRTM3 abolishes surface expression of the AMPA receptor GluA1 subunit after cLTP induction (Figure 3), showing that LRRTM3 also contributes to the maintenance of surface GluA1. Strikingly, re-expression of the LRRTM3 L3S variant (which interacts with PSD-95), but not L3L or L3S VA (which do not interact with PSD-95), restored the deficit in activity-induced surface GluA1 upregulation caused by LRRTM3 loss (Figure 3). Consistent with this finding, deletion of LRRTM3 proteins mildly decreased LTP in PP-to-DG synapses (Figure S6E). These data suggest that LRRTM3 controls the activity-dependent regulation of surface AMPA receptor trafficking (i.e., exocytosis and/or endocytosis) through its PSD-95 interaction, possibly involving the PSD-95/TARP complex (Nicoll et al., 2006), and further implies that other LRRTMs may act similarly. It remains to be determined whether presynaptic neurexins are also involved in LRRTM3-mediated postsynaptic AMPA receptor trafficking, and which intracellular alternative splicing machineries operate on LRRTM3, as well as LRRTM4. One mechanism that might plausibly control alternative splicing is specific synaptic activity, reminiscent of situation with neurexin alternative splicing (Aoto et al., 2013; Iijima et al., 2011).
4. Analyses with Lrrtm3-KO mice revealed that LRRTM3 is specifically required for excitatory synapse structure and function in DG granule neurons, but not in CA1 pyramidal neurons, in vivo. Although gross synapse morphology was unchanged in Lrrtm3-KO brains, Golgi staining, electron microscopy, and quantitative confocal microscopy revealed that excitatory synapse numbers were reduced (Figures 4 and 5). In accord with these structural defects in Lrrtm3-KO brains, excitatory synaptic transmission was also selectively impaired in DG granule neurons (Figure 6). The amplitude of sEPSCs and mEPSCs and excitability were significantly reduced, whereas the frequency of mEPSCs (but not that of sEPSCs) was unexpectedly increased (Figures 6A–6E). In support of the increase in mEPSC frequency in Lrrtm3-KO, the paired-pulse ratio at a 20-ms interstimulus interval was decreased in

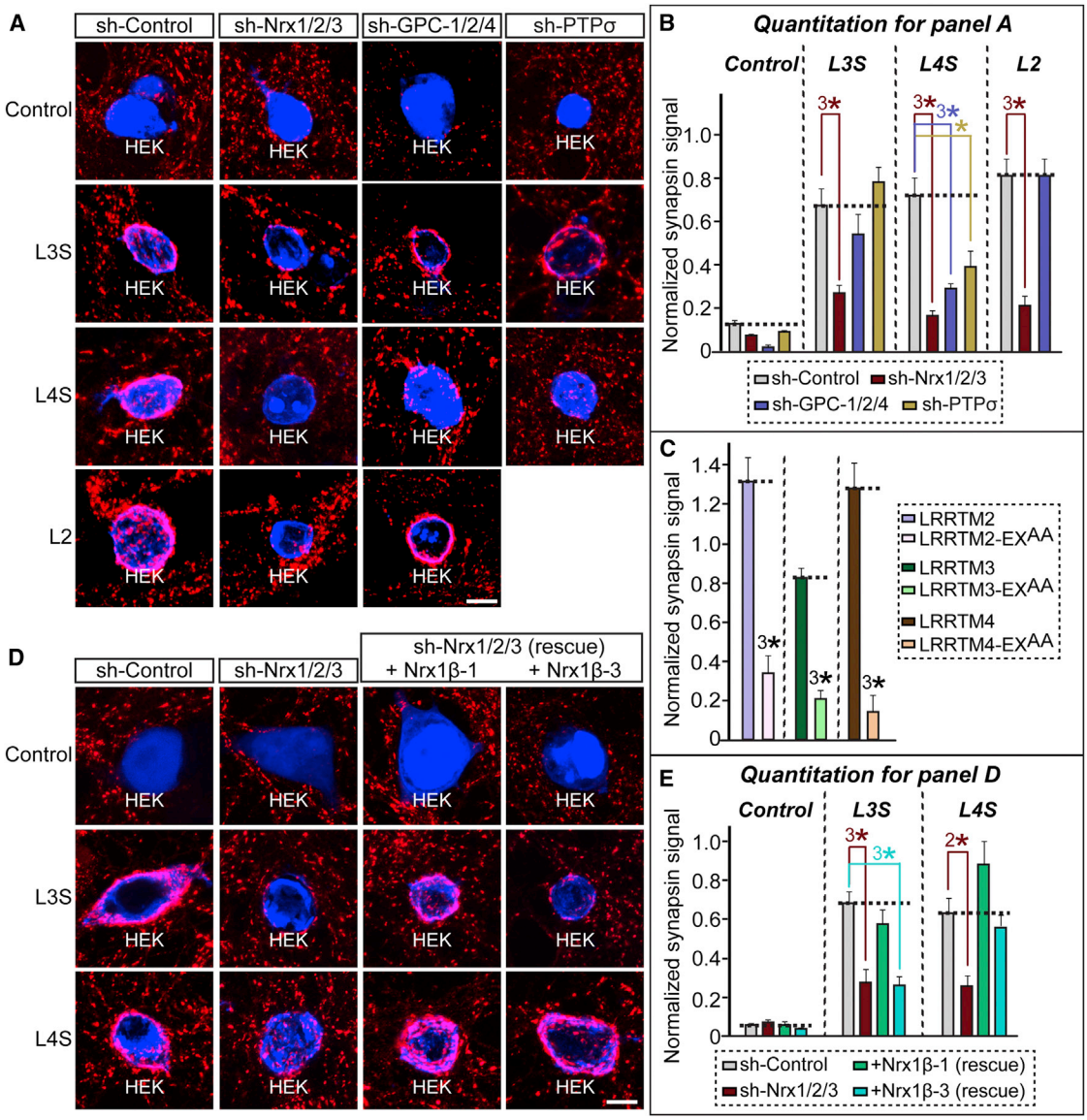

Figure 7. Presynaptic Neurexins Are Required for LRRTM3-mediated Presynaptic Differentiation

(A and B) The effect of triple neurexin knockdown (sh-Nrx1/2/3), triple GPC knockdown (sh-GPC-1/2/4), or single PTPσ knockdown on the synaptogenic activities of LRRTM3 (L3S), LRRTM4 (L4S), and LRRTM2 (L2). Representative images (A) of cocultures immunostained with antibodies to mVenus or HA (blue) and synapsin (red). Coincident signals are indicated in violet. Scale bar represents 20 μm (applies to all images). Quantitation (B) of heterologous synapse-formation assays, measured as the ratio of synapsin to EGFP/HA fluorescence signals. The dashed lines correspond to control values used as a baseline. Data shown are means ± SEMs ($^{3*}p < 0.001$ and $^{*}p < 0.05$, ANOVA with Tukey's test; n denotes the total number of HEK293T cells analyzed as follows: sh-Control/Control, n = 11; sh-Control/L3S, n = 20; sh-Control/L4S, n = 12; sh-Control/L2, n = 11; sh-Nrx1/2/3/Control, n = 11; sh-Nrx1/2/3/L3S, n = 28; sh-Nrx1/2/3/L4S, n = 12; sh-Nrx1/2/3/L2, n = 11; sh-GPC-1/2/4/Control, n = 10; sh-GPC-1/2/4/L3S, n = 10; sh-GPC-1/2/4/L4S, n = 11; sh-GPC-1/2/4/L2, n = 10; sh-PTPσ/Control, n = 11; sh-PTPσ/L3S, n = 13; and sh-PTPσ/L4S, n = 13).

(C) Summary graphs of heterologous synapse-formation assays examining the effects of point mutations on the synaptogenic activities of LRRTMs. Point mutants of LRRTM2, LRRTM3, and LRRTM4 (LRRTM2-EX^{AA}, LRRTM3-EX^{AA} and LRRTM4-EX^{AA}, respectively; EX, extracellular; AA, replaced with double alanines) exhibited significantly reduced synaptogenic activities compared to the corresponding WT protein. For representative images for experiments, see Figure S7D. The dashed lines correspond to control values used as a baseline. Data shown are means ± SEMs ($^{3*}p < 0.001$, Student's t test; n denotes the total number of HEK293T cells analyzed as follows: LRRTM2, n = 10; LRRTM2-EX^{AA}, n = 11; LRRTM3, n = 10; LRRTM3-EX^{AA}, n = 12; LRRTM4, n = 13; and LRRTM4-EX^{AA}, n = 12).

(D and E) Further analysis of the effects of triple neurexin knockdown (sh-Nrx1/2/3) on the synaptogenic activities of LRRTM3 (L3S) and LRRTM4 (L4S). HEK293T cells expressing EGFP alone (Control), HA-L3S, or HA-L4S were cocultured with neurons infected with control lentiviruses (sh-Control) or lentiviruses expressing sh-Nrx1/2/3, without or with coexpression of Nrx1β splice variants as indicated (+Nrx1β-1 or +Nrx1β-3). Representative images (D) and summary graphs (E) for heterologous synapse-formation assays are presented. The dashed lines correspond to control values used as a baseline. Data shown are means ± SEMs

(legend continued on next page)

Lrrtm3-KO mice (Figures 6I and 6J). Collectively, these data suggest the operation of a possible compensatory mechanism and further indicate that the tetrodotoxin (TTX)-sensitive component of excitatory synaptic transmission is markedly inactive whereas the TTX-resistant component is hyperactive. Thus, the net effect of the loss of LRRTM3 proteins is a reduction in sEPSCs. Alternatively, it is possible that a decreased network activity in LRRTM3-deficient brains activates homeostasis mechanisms, increasing the mEPSC frequency. Regardless of the precise mechanisms, our results unequivocally demonstrated that all four LRRTMs are critical for excitatory synapse development.

5. Finally, we found that neurexins are equally important for all LRRTM family proteins in mediating presynaptic differentiation, at least in heterologous synapse-formation assays (Figure 7). Triple KD of neurexins completely abolished the synaptogenic activity of LRRTM2 and LRRTM3 and partially decreased the synaptogenic activity of LRRTM4, suggesting that neurexins are required for the synaptogenic activity of all LRRTM proteins (Figures 7A and 7B). In support of this interpretation, point mutants of LRRTM2, -3, and -4 that are predicted to disrupt neurexin-binding lacked synapse-inducing activity (Figures 7C, S8C, and S8D). However, different sets of presynaptic neurexins are involved in LRRTM activities. For example, LRRTM2 and LRRTM3 selectively formed complexes with only #SS4-negative splice variants of neurexins, whereas LRRTM4 induction of presynaptic differentiation was linked to both #SS4-negative and positive splice variants of neurexins (Figures 7D, 7E, and S7B; see de Wit et al., 2013). Triple KD of hippocampal GPCs and KD of PTPσ also partially decreased the synaptogenic activity of LRRTM4 (Figures 7A and 7B), consistent with a previous report (Ko et al., 2015b). Collectively, these data indicate that presynaptic neurexins are bona fide ligands for LRRTMs and that GPCs act as additional ligands for LRRTM4, although the functional significance of this latter observation will require further investigation.

In summary, our data consistently support the conclusion that LRRTM3 is critical for excitatory synapse development and function in hippocampal DG. The functional properties of LRRTM3 are similar to those of other LRRTMs in that LRRTM3 specifically acts in promoting excitatory synapse development, maintains surface AMPA receptor levels, and interacts with presynaptic neurexins. In particular, various phenotypes of Lrrtm3-KO mice are similar to those reported for Lrrtm4-KO mice (Siddiqui et al., 2013). Intriguingly, both LRRTM3 and LRRTM4, together with neurexins and GPCs, have been implicated in ASDs (Michaelson et al., 2012; Pinto et al., 2010), suggesting that these molecular complexes contribute to ASD pathophysiology. In keeping with this concept, our current results support the use of Lrrtm3-KO mice as a tool for subsequent studies designed to develop effective therapeutic avenues for ASDs.

EXPERIMENTAL PROCEDURES

Antibodies

LRRTM3[Long] peptide (JK092; CDLSTITSAGRISDHKPQLA) was synthesized and conjugated to keyhole limpet hemocyanin through a cysteine added to the N terminus of the peptide. Other antibodies were obtained commercially as detailed in the Supplemental Experimental Procedures.

Production of Lentiviruses

Recombinant lentiviruses were produced by triply transfecting HEK293T cells with three plasmids—various L-309 or L-313 vectors, psPAX, and pMD2G—using FuGene-6 (Roche) as previously described (Ko et al., 2015b). Cultured rat hippocampal neurons were infected at DIV3 and harvested at DIV12–13. Knockdown efficacy was measured using qRT-PCR, as previously described (Lee et al., 2013).

Cultured Neuron Preparation, Transfections, Imaging, and Quantifications

Cultured hippocampal neurons were prepared from E18 rat brain, as previously described (Ko et al., 2006a, 2006b). For overexpression or KD of LRRTM3 proteins in cultured neurons, hippocampal neurons were transfected using a CalPhos Kit (Clontech) at DIV8–10 and immunostained at DIV14.

Electrophysiology

WT and Lrrtm3-KO mice (2 to 5 weeks old) were used in electrophysiological experiments. The significance of differences between two groups was determined using Student's t test or Mann-Whitney *U* test.

Heterologous Synapse-Formation Assays

HEK293T cells were transfected with pDisplay-LRRTM2 (HA-L2), pDisplay-LRRTM3 (HA-L3L and HA-L3S), pDisplay-LRRTM4 (HA-L4L and HA-L4S), or EGFP (Control) using FuGene (Roche). Heterologous synapse-formation assays were performed as previously described (Um et al., 2014a). For the experiments presented in Figure 7, cultured hippocampal neurons were infected at DIV3 with lentiviruses expressing shRNAs, as indicated, and incubated until transfected HEK293T cells were added at DIV10 for synapse-formation assays.

Statistics

All data are expressed as mean ± SEM. All experiments were repeated with at least three independent cultures and evaluated statistically using ANOVA with post hoc Tukey's test or Student's t test.

Full experimental procedures and associated references are available in the Supplemental Information.

SUPPLEMENTAL INFORMATION

Supplemental Information includes Supplemental Experimental Procedures, seven figures, and two tables and can be found with this article online at http://dx.doi.org/10.1016/j.celrep.2015.12.081.

AUTHOR CONTRIBUTIONS

J.K. designed and supervised the project. T.-Y.C. and S.-Y.C. performed electrophysiology recordings. H. Kang performed cell biology experiments and quantitative image analyses. D.P. performed biochemistry experiments. G.C. performed cell biology experiments and supervised maintenance of Lrrtm3-KO mice. Y.S.C. and Y.-C.B. performed electron microscopy experiments.

($^{3*}p < 0.001$ and $^{2*}p < 0.01$, ANOVA with Tukey's test; n denotes the total number of HEK293T cells analyzed as follows: sh-Control/Control, n = 10; sh-Nrx1/2/3/Control, n = 10; sh-Nrx1/2/3 (rescue + Nrx1β-1)/Control, n = 10; sh-Nrx1/2/3 (rescue + Nrx1β-3)/Control, n = 10; sh-Control/L3S, n = 12; sh-Nrx1/2/3/L3S, n = 10; sh-Nrx1/2/3 (rescue + Nrx1β-1)/L3S, n = 13; sh-Nrx1/2/3 (rescue + Nrx1β-3)/L3S, n = 14; sh-Control/L4S, n = 10; sh-Nrx1/2/3/L4S, n = 12; sh-Nrx1/2/3 (rescue + Nrx1β-1)/L4S, n = 11; and sh-Nrx1/2/3 (rescue + Nrx1β-3)/L4S, n = 12. Scale bar represents 20 μm (applies to all images).

P.U. and M.S.A. performed qRT-PCR experiments and provided Lrrtm3-KO mice. D.L. and H. Kim performed in situ hybridization analyses. D.C. and S.-H.L. performed Nissl staining. S.J. contributed to generating key reagents. J.W.U. performed the remaining experiments. J.W.U. and J.K. wrote the manuscript.

ACKNOWLEDGMENTS

This work was supported by grants from the National Research Foundation of Korea (NRF) funded by the Ministry of Science and Future Planning (2014051826 to J.K. and S.-H.L., 2014047939 to H. Kim, and MISP, 2008-0062282 to Y.-C.B.), the Yonsei University Future-leading Research Initiative of 2014 (to J.K.), the Yonsei University Future-leading Research Initiative of 2015 (to J.W.U.), a new faculty research seed money grant of Yonsei University College of Medicine for 2015 (2015-32-0019 to J.W.U.), the NRF funded by the Ministry of Education, Science and Technology (NRF-2013R1A6A3A04061338 to J.W.U.), the Sigrid Juselius Foundation (to M.S.A.), the Academy of Finland (to P.U.), and in part by the Brain Korea 21 (BK21) PLUS program. H. Kang, G.C., D.P., and S.J. are fellowship awardees of the BK21 PLUS program.

Received: August 3, 2015
Revised: October 29, 2015
Accepted: December 16, 2015
Published: January 14, 2016

REFERENCES

Aoto, J., Martinelli, D.C., Malenka, R.C., Tabuchi, K., and Südhof, T.C. (2013). Presynaptic neurexin-3 alternative splicing trans-synaptically controls postsynaptic AMPA receptor trafficking. Cell *154*, 75–88.

de Wit, J., and Ghosh, A. (2014). Control of neural circuit formation by leucine-rich repeat proteins. Trends Neurosci. *37*, 539–550.

de Wit, J., Sylwestrak, E., O'Sullivan, M.L., Otto, S., Tiglio, K., Savas, J.N., Yates, J.R., 3rd, Comoletti, D., Taylor, P., and Ghosh, A. (2009). LRRTM2 interacts with Neurexin1 and regulates excitatory synapse formation. Neuron *64*, 799–806.

de Wit, J., O'Sullivan, M.L., Savas, J.N., Condomitti, G., Caccese, M.C., Vennekens, K.M., Yates, J.R., 3rd, and Ghosh, A. (2013). Unbiased discovery of glypican as a receptor for LRRTM4 in regulating excitatory synapse development. Neuron *79*, 696–711.

Dresbach, T., Neeb, A., Meyer, G., Gundelfinger, E.D., and Brose, N. (2004). Synaptic targeting of neuroligin is independent of neurexin and SAP90/PSD95 binding. Mol. Cell. Neurosci. *27*, 227–235.

Gokce, O., and Südhof, T.C. (2013). Membrane-tethered monomeric neurexin LNS-domain triggers synapse formation. J. Neurosci. *33*, 14617–14628.

Iijima, T., Wu, K., Witte, H., Hanno-Iijima, Y., Glatter, T., Richard, S., and Scheiffele, P. (2011). SAM68 regulates neuronal activity-dependent alternative splicing of neurexin-1. Cell *147*, 1601–1614.

Kim, S., Burette, A., Chung, H.S., Kwon, S.K., Woo, J., Lee, H.W., Kim, K., Kim, H., Weinberg, R.J., and Kim, E. (2006). NGL family PSD-95-interacting adhesion molecules regulate excitatory synapse formation. Nat. Neurosci. *9*, 1294–1301.

Ko, J. (2012). The leucine-rich repeat superfamily of synaptic adhesion molecules: LRRTMs and Slitrks. Mol. Cells *34*, 335–340.

Ko, J., Kim, S., Chung, H.S., Kim, K., Han, K., Kim, H., Jun, H., Kaang, B.K., and Kim, E. (2006a). SALM synaptic cell adhesion-like molecules regulate the differentiation of excitatory synapses. Neuron *50*, 233–245.

Ko, J., Yoon, C., Piccoli, G., Chung, H.S., Kim, K., Lee, J.R., Lee, H.W., Kim, H., Sala, C., and Kim, E. (2006b). Organization of the presynaptic active zone by ERC2/CAST1-dependent clustering of the tandem PDZ protein syntenin-1. J. Neurosci. *26*, 963–970.

Ko, J., Fuccillo, M.V., Malenka, R.C., and Südhof, T.C. (2009). LRRTM2 functions as a neurexin ligand in promoting excitatory synapse formation. Neuron *64*, 791–798.

Ko, J., Soler-Llavina, G.J., Fuccillo, M.V., Malenka, R.C., and Südhof, T.C. (2011). Neuroligins/LRRTMs prevent activity- and Ca2+/calmodulin-dependent synapse elimination in cultured neurons. J. Cell Biol. *194*, 323–334.

Ko, J., Choii, G., and Um, J.W. (2015a). The balancing act of GABAergic synapse organizers. Trends Mol. Med. *21*, 256–268.

Ko, J.S., Pramanik, G., Um, J.W., Shim, J.S., Lee, D., Kim, K.H., Chung, G.Y., Condomitti, G., Kim, H.M., Kim, H., et al. (2015b). PTPσ functions as a presynaptic receptor for the glypican-4/LRRTM4 complex and is essential for excitatory synaptic transmission. Proc. Natl. Acad. Sci. USA *112*, 1874–1879.

Laakso, T., Muggalla, P., Kysenius, K., Laurén, J., Paatero, A., Huttunen, H.J., and Airaksinen, M.S. (2012). LRRTM3 is dispensable for amyloid-β production in mice. J. Alzheimers Dis. *31*, 759–764.

Laurén, J., Airaksinen, M.S., Saarma, M., and Timmusk, T. (2003). A novel gene family encoding leucine-rich repeat transmembrane proteins differentially expressed in the nervous system. Genomics *81*, 411–421.

Lee, K., Kim, Y., Lee, S.J., Qiang, Y., Lee, D., Lee, H.W., Kim, H., Je, H.S., Südhof, T.C., and Ko, J. (2013). MDGAs interact selectively with neuroligin-2 but not other neuroligins to regulate inhibitory synapse development. Proc. Natl. Acad. Sci. USA *110*, 336–341.

Linhoff, M.W., Laurén, J., Cassidy, R.M., Dobie, F.A., Takahashi, H., Nygaard, H.B., Airaksinen, M.S., Strittmatter, S.M., and Craig, A.M. (2009). An unbiased expression screen for synaptogenic proteins identifies the LRRTM protein family as synaptic organizers. Neuron *61*, 734–749.

Michaelson, J.J., Shi, Y., Gujral, M., Zheng, H., Malhotra, D., Jin, X., Jian, M., Liu, G., Greer, D., Bhandari, A., et al. (2012). Whole-genome sequencing in autism identifies hot spots for de novo germline mutation. Cell *151*, 1431–1442.

Minatohara, K., Murata, Y., Fujiyoshi, Y., and Doi, T. (2015). An intracellular domain with a novel sequence regulates cell surface expression and synaptic clustering of leucine-rich repeat transmembrane proteins in hippocampal neurons. J. Neurochem. *134*, 618–628.

Missler, M., Südhof, T.C., and Biederer, T. (2012). Synaptic cell adhesion. Cold Spring Harb. Perspect. Biol. *4*, a005694.

Nicoll, R.A., Tomita, S., and Bredt, D.S. (2006). Auxiliary subunits assist AMPA-type glutamate receptors. Science *311*, 1253–1256.

Pinto, D., Pagnamenta, A.T., Klei, L., Anney, R., Merico, D., Regan, R., Conroy, J., Magalhaes, T.R., Correia, C., Abrahams, B.S., et al. (2010). Functional impact of global rare copy number variation in autism spectrum disorders. Nature *466*, 368–372.

Schwenk, J., Harmel, N., Brechet, A., Zolles, G., Berkefeld, H., Müller, C.S., Bildl, W., Baehrens, D., Hüber, B., Kulik, A., et al. (2012). High-resolution proteomics unravel architecture and molecular diversity of native AMPA receptor complexes. Neuron *74*, 621–633.

Shanks, N.F., Savas, J.N., Maruo, T., Cais, O., Hirao, A., Oe, S., Ghosh, A., Noda, Y., Greger, I.H., Yates, J.R., 3rd, and Nakagawa, T. (2012). Differences in AMPA and kainate receptor interactomes facilitate identification of AMPA receptor auxiliary subunit GSG1L. Cell Rep. *1*, 590–598.

Siddiqui, T.J., Pancaroglu, R., Kang, Y., Rooyakkers, A., and Craig, A.M. (2010). LRRTMs and neuroligins bind neurexins with a differential code to cooperate in glutamate synapse development. J. Neurosci. *30*, 7495–7506.

Siddiqui, T.J., Tari, P.K., Connor, S.A., Zhang, P., Dobie, F.A., She, K., Kawabe, H., Wang, Y.T., Brose, N., and Craig, A.M. (2013). An LRRTM4-HSPG complex mediates excitatory synapse development on dentate gyrus granule cells. Neuron *79*, 680–695.

Soler-Llavina, G.J., Fuccillo, M.V., Ko, J., Südhof, T.C., and Malenka, R.C. (2011). The neurexin ligands, neuroligins and leucine-rich repeat transmembrane proteins, perform convergent and divergent synaptic functions in vivo. Proc. Natl. Acad. Sci. USA *108*, 16502–16509.

Soler-Llavina, G.J., Arstikaitis, P., Morishita, W., Ahmad, M., Südhof, T.C., and Malenka, R.C. (2013). Leucine-rich repeat transmembrane proteins are essential for maintenance of long-term potentiation. Neuron *79*, 439–446.

Südhof, T.C. (2008). Neuroligins and neurexins link synaptic function to cognitive disease. Nature *455*, 903–911.

Takahashi, H., and Craig, A.M. (2013). Protein tyrosine phosphatases PTPδ, PTPσ, and LAR: presynaptic hubs for synapse organization. Trends Neurosci. *36*, 522–534.

Takashima, N., Odaka, Y.S., Sakoori, K., Akagi, T., Hashikawa, T., Morimura, N., Yamada, K., and Aruga, J. (2011). Impaired cognitive function and altered hippocampal synapse morphology in mice lacking Lrrtm1, a gene associated with schizophrenia. PLoS ONE *6*, e22716.

Um, J.W., and Ko, J. (2013). LAR-RPTPs: synaptic adhesion molecules that shape synapse development. Trends Cell Biol. *23*, 465–475.

Um, J.W., Kim, K.H., Park, B.S., Choi, Y., Kim, D., Kim, C.Y., Kim, S.J., Kim, M., Ko, J.S., Lee, S.G., et al. (2014a). Structural basis for LAR-RPTP/Slitrk complex-mediated synaptic adhesion. Nat. Commun. *5*, 5423.

Um, J.W., Pramanik, G., Ko, J.S., Song, M.Y., Lee, D., Kim, H., Park, K.S., Südhof, T.C., Tabuchi, K., and Ko, J. (2014b). Calsyntenins function as synaptogenic adhesion molecules in concert with neurexins. Cell Rep. *6*, 1096–1109.

Voikar, V., Kulesskaya, N., Laakso, T., Lauren, J., Strittmatter, S.M., and Airaksinen, M.S. (2013). LRRTM1-deficient mice show a rare phenotype of avoiding small enclosures–a tentative mouse model for claustrophobia-like behaviour. Behav. Brain Res. *238*, 69–78.

Yim, Y.S., Kwon, Y., Nam, J., Yoon, H.I., Lee, K., Kim, D.G., Kim, E., Kim, C.H., and Ko, J. (2013). Slitrks control excitatory and inhibitory synapse formation with LAR receptor protein tyrosine phosphatases. Proc. Natl. Acad. Sci. USA *110*, 4057–4062.